Electronic Supplementary Material (ESI) for New Journal of Chemistry.

SUPPORTING INFORMATION

Electrode-free flexible batteries enabled by electro-depositing both Zn and MnO_2 from electrolytes

Shiqiang Luo [a,] †*, Shiwei Liu [a,] †, Guoshen Yang [b], Chuanlong Liu [c], Jiazhen Wu [c], Pritesh Hiralal [a]*, Zanxiang Nie [a], Gehan A.J. Amaratunga [a] and Hang Zhou [b]*

[a] Zinergy Shenzhen Ltd., Gangzhilong Science Park, Shenzhen, Guangdong, China.

[b] School of Electronic and Computer Engineering, Peking University Shenzhen Graduate School, Shenzhen, Guangdong, China.

[c] Department of Materials Science and Engineering, Southern University of Science and Technology, 518055, Shenzhen, China

† These authors contributed equally to this work

*Corresponding author. E-mail: luoshiqiang@zinergy-power.cn (S. Luo), pritesh@zinergy-power.com (P. Hiralal), zhouh81@pkusz.edu.cn (H. Zhou)

Experimental

1. Materials

Zinc acetate dehydrate ($ZnAc_2 \cdot 2H_2O$), manganese acetate tetrahydrate ($MnAc_2 \cdot 4H_2O$), KCl, and KI were purchased from Aladdin China with analytical reagent grade. The zinc foils (0.3 mm thickness), graphite felts (3 mm thickness), carbon fiber ropes (2 mm diameter) and filter papers (0.17mm thickness) were all purchased from Taobao and used without special treatment. The thin-film electrodes were produced by Zinergy Shenzhen Ltd. by screen-printing method. Polyethylene terephthalate (PET) is used as substrate. The printable carbon/zinc/MnO_2 paste was prepared by mixing graphite/zinc powder/electrolytic MnO_2 powder, carbon black, polymer binder, and solvent. The printable pastes were annealed at 100 ℃ after screen-printing, where the zinc and MnO_2 pastes were printed onto the annealed carbon layers. The thickness of the carbon, zinc and MnO_2 layers were controlled to be 10, 50 and 80 μm, respectively.

2. Battery Fabrication and characterization

For the cuvette batteries, 5mL-size cuvettes were used as containers, graphite felts or zinc foils and graphite felts were used for anodes and cathode current collectors, respectively. The size of the active, exposed areas was 1 × 2 cm^2, and these were placed at opposite faces of the cuvette, with a piece of filter paper loosely in between acting as a separator. 3 mL electrolyte was added to complete the cell, which was then sealed with scotch tape. The charge and discharge curves were measured by a LANHE CT3002AU battery tester. The cuvette batteries were charged and discharged under 10 mA current with the charge capacity fixed at 5 mAh.

For thin-film batteries, current collectors consisted of screen-printed carbon films onto which the anode/cathode layers where either printed or electrolytically deposited during cell charge. Filter papers were inserted between the anode and cathode as separators and 250 μL electrolyte was added with a micro-pipette before sealing.

These cells had an active electrode area of 4 × 2.5 cm^2. The batteries were charged and discharged under 2 mA current.

For cable batteries, two carbon ropes were cut to a length of 6 cm, and one of these was wrapped with filter paper. Then, the wrapped carbon rope was wound with the un-wrapped one and wrapped in cling film after adding 600 μL starch-gel electrolyte in-between. The starch-gel electrolytes were made by adding 20% (20 g in 100 mL) starch into the 1 **M** $ZnAc_2$ + 1 **M** $MnAc_2$ + 0.1 **M** KI + 2 **M** KCl electrolyte (**M**: mole per liter) and annealing at 90 ℃ for 20 mins. Then, the rolled cable batteries were put into heat shrink sleeves and shrunk tight using a hot air gun. Hot melt adhesives were used to seal the two ends. The diameter of final cable batteries was 0.46 cm. The batteries were charged and discharged under 2 mA current.

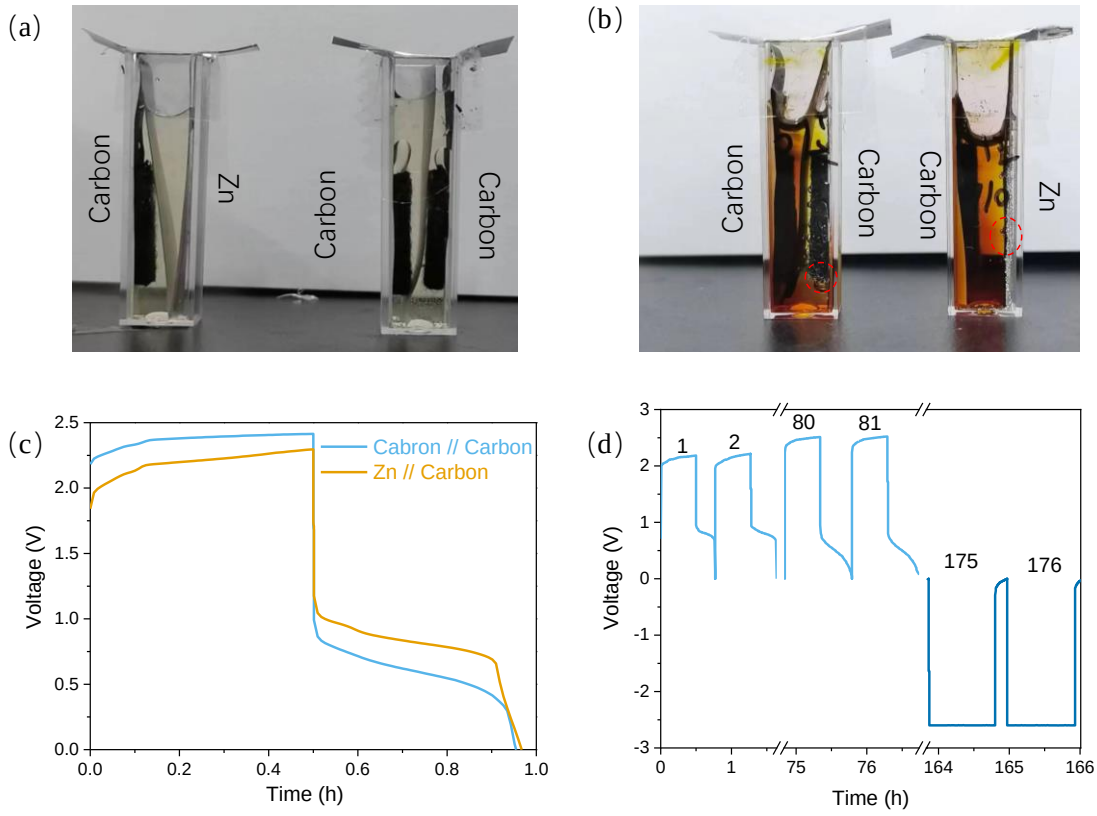

Fig. S1. The photo of the cuvette batteries (a) before cycling and (b) after cycling, where the hydrogen bubbles were marked by red dashed line. The voltage curves of (b) the carbon//carbon and zinc//carbon at the 50th cycle and (c) the carbon//carbon under different cycle numbers in Fig. 1(b).

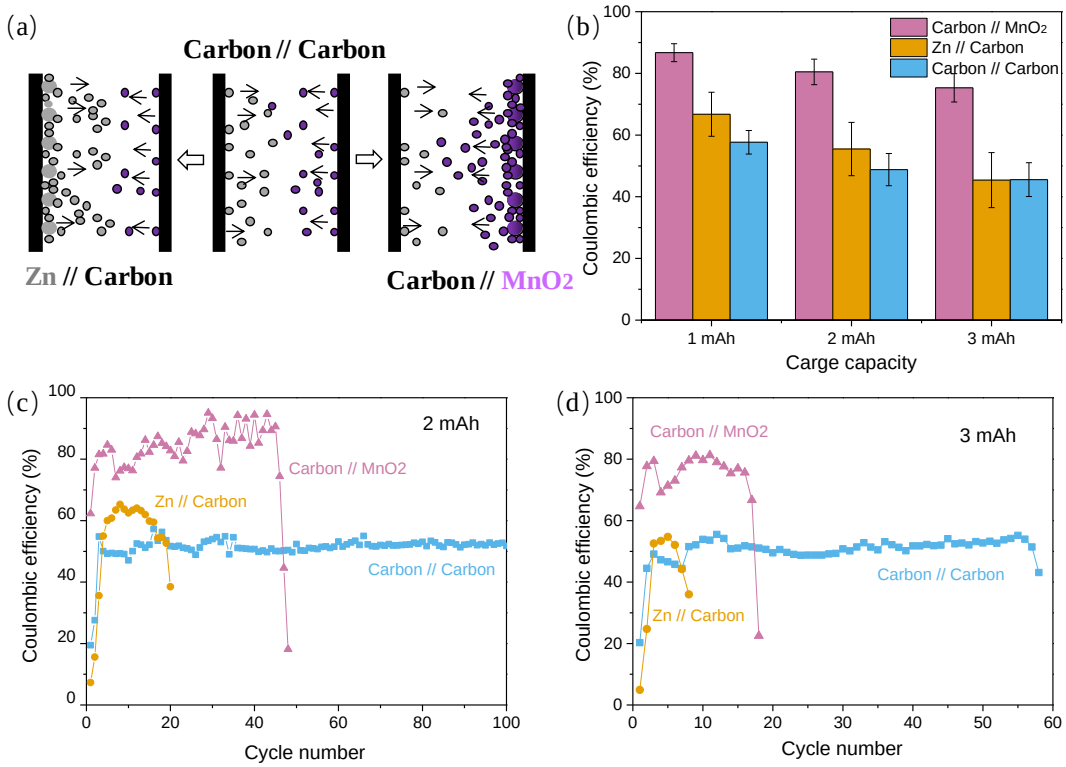

Fig. S2. The scheme (a) and CEs summary (b) of the thin-film batteries (based on Zn//carbon, carbon//carbon and carbon//MnO_2) under 2 mA charge/discharge currents. The cycling performance of with charge capacity fixed at (c) 2 mAh and (d) 3 mAh. The electrolytes were all composed of 1 **M** $ZnAc_2$ + 1 **M** $MnAc_2$ + 0.1 **M** KI + 2 **M** KCl.

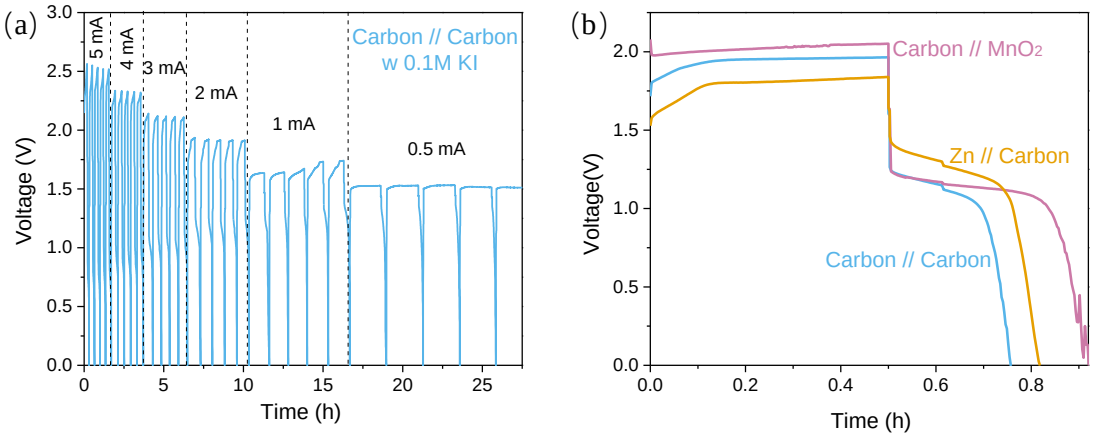

Fig. S3. (a) The voltage curves of the thin-film batteries based on carbon//carbon electrodes under different charge/discharge currents (0.5~5 mA) with charge capacity fixed at 1 mAh. (b) The voltage curves at the 50th cycle in Fig. 2(b) of thin-film batteries based on Zn//carbon, carbon//carbon and carbon//MnO_2, where the charge/discharge currents were set to 2 mA and the charge capacities were fixed at 1 mAh. The electrolytes were composed of 1 **M** $ZnAc_2$ + 1 **M** $MnAc_2$ + 0.1 **M** KI + 2 **M** KCl. The 2-mA charge/discharge current was selected in order to avoid high charging voltage (cut-off at 2.6 V) which may cause hydrogen evolution.

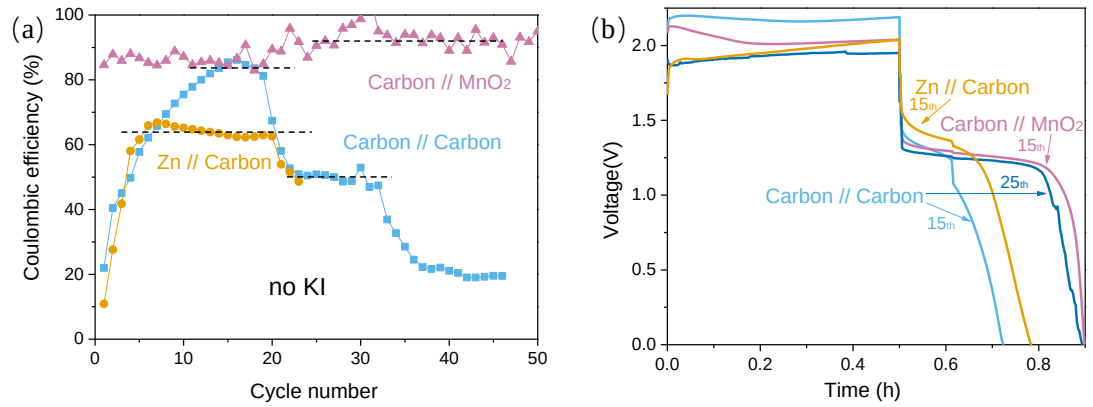

Fig. S4. (a) The CEs and (b) voltage curves of the thin-film batteries (based on Zn//carbon, carbon//carbon and carbon//MnO_2) under 2 mA charge/discharge currents with charge capacity fixed at 1 mAh. The electrolytes were composed of 1 **M** $ZnAc_2$ + 1 **M** $MnAc_2$ + 2 **M** KCl.

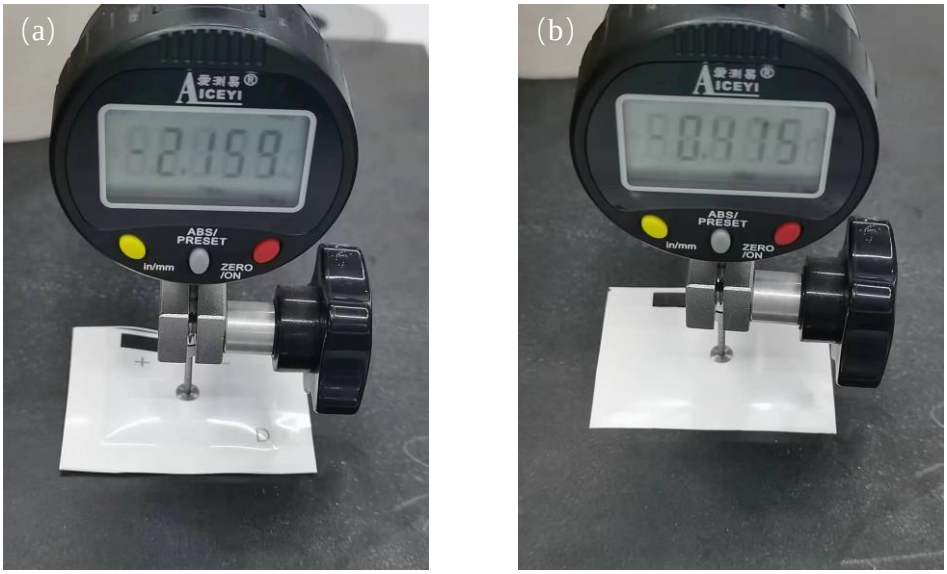

Fig. S5. The thickness measurement of the thin-film batteries based on (a) Zn//carbon and (b) carbon//carbon, which is 2.159 and 0.415 mm, respectively.

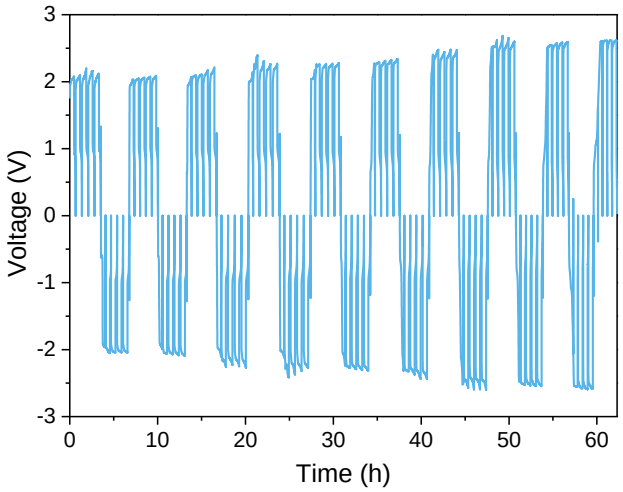

Fig. S6. Voltage curves of the thin-film batteries based on printed carbon//carbon films with charge/discharge electrodes reversed after every 5 cycles.

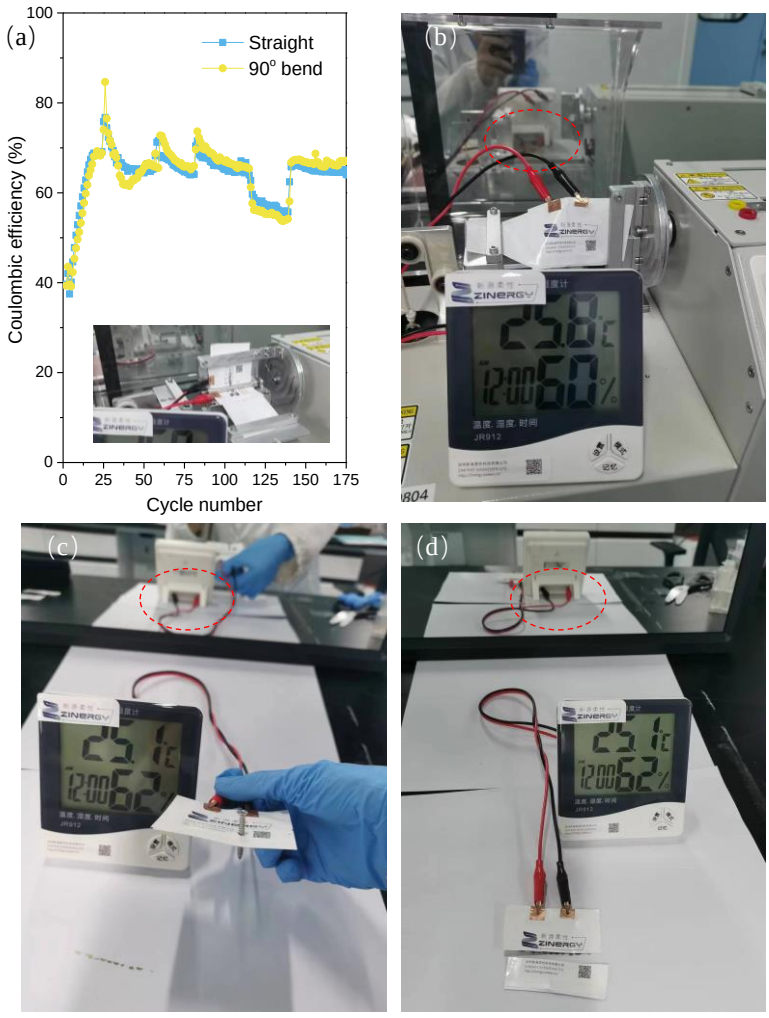

Fig. S7. (a) The CEs of the thin-film carbon//carbon batteries with and without 90° bending, where the photo of bent battery is shown in the inset. Demonstration of flexibility and safety of the thin-film carbon//carbon batteries by (b) twisting, (c) nailing and (d) cutting, where a mirror was put behind to prove the direct connection to the digital display meter. The electrolytes for the batteries were composed of 1 **M** $ZnAc_2$ + 1 **M** $MnAc_2$ + 0.1 **M** KI + 2 **M** KCl. Machine measurement instability caused the oscillation in (a).

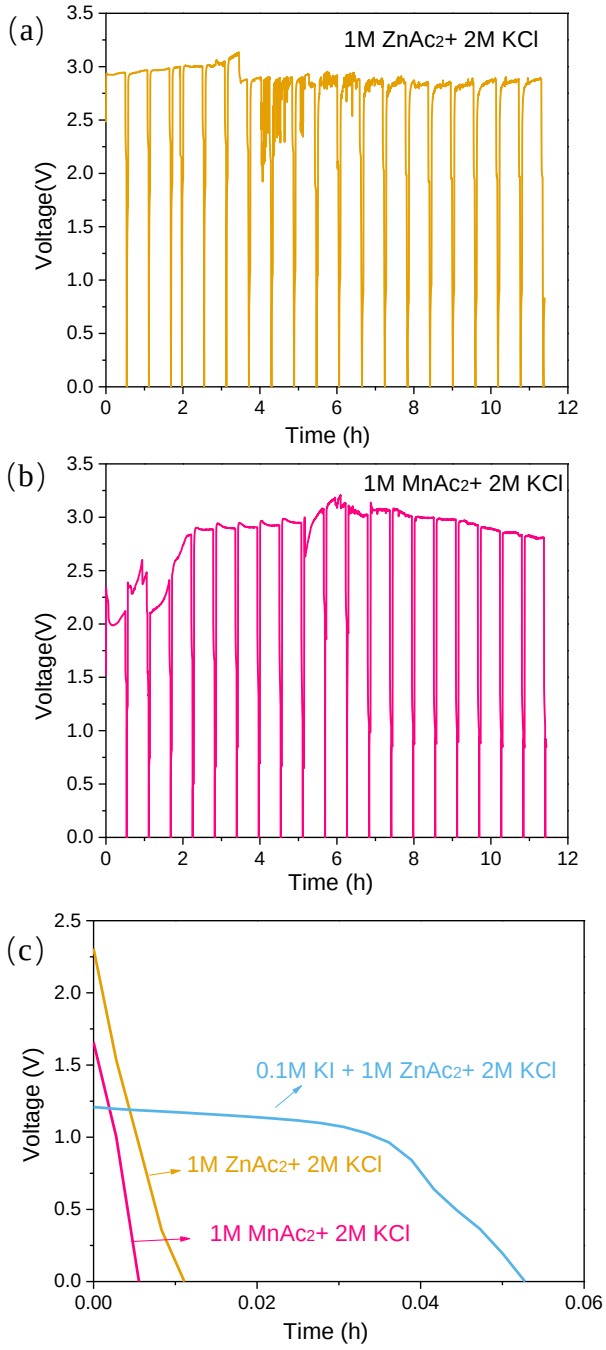

Fig. S8. The voltage curves of the thin-film carbon//carbon batteries based on electrolytes of (a) 1 **M** $ZnAc_2$ + 2 **M** KCl and (b) 1 **M** $MnAc_2$ + 2 **M** KCl. (c) Discharge curves in (a-b) were compared with batteries based on 1 **M** $ZnAc_2$ + 0.1 **M** KI + 2 **M** KCl. The charge/discharge currents were 2 mA and the charge capacities were fixed at 1 mAh.

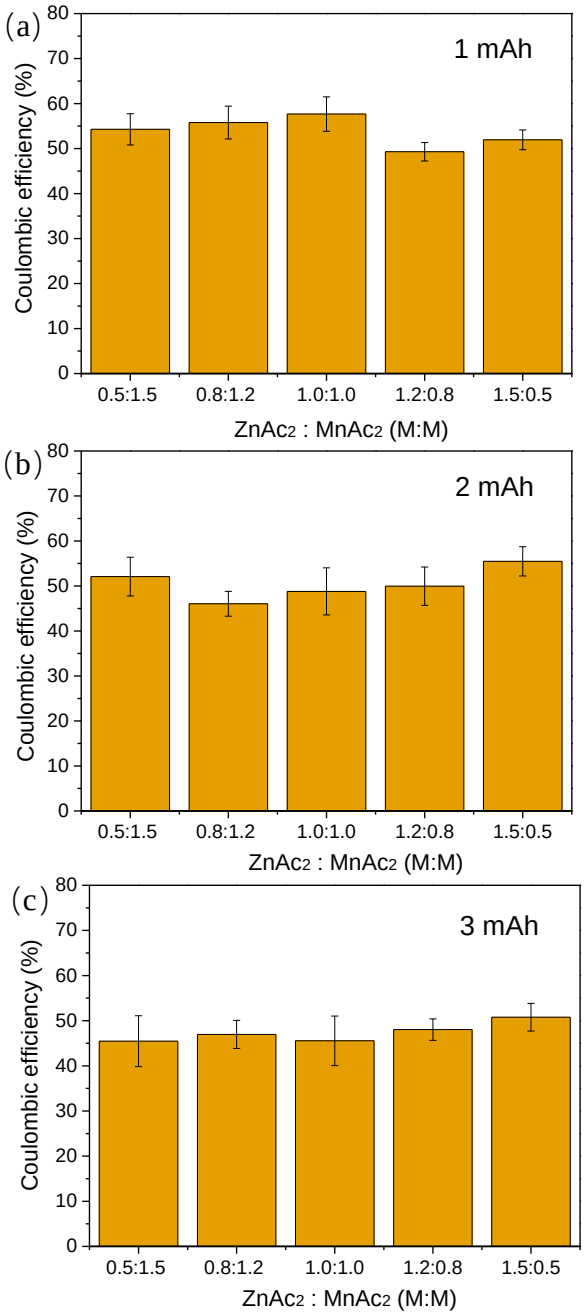

Fig. S9. The CEs of the thin-film carbon//carbon batteries based on electrolytes of x **M** $ZnAc_2$ + y **M** $MnAc_2$ + 0.1 **M** KI + 2 **M** KCl under 2 mA charge/discharge currents with charge capacity fixed as (a) 1 mAh, (b) 2 mAh and (c) 3 mAh. The (x, y) = (0.5, 1.5), (0.8, 1.2), (1.0, 1.0), (1.2, 0.8) and (1.5, 0.5), which were limited by the solubility of $ZnAc_2$ and $MnAc_2$.

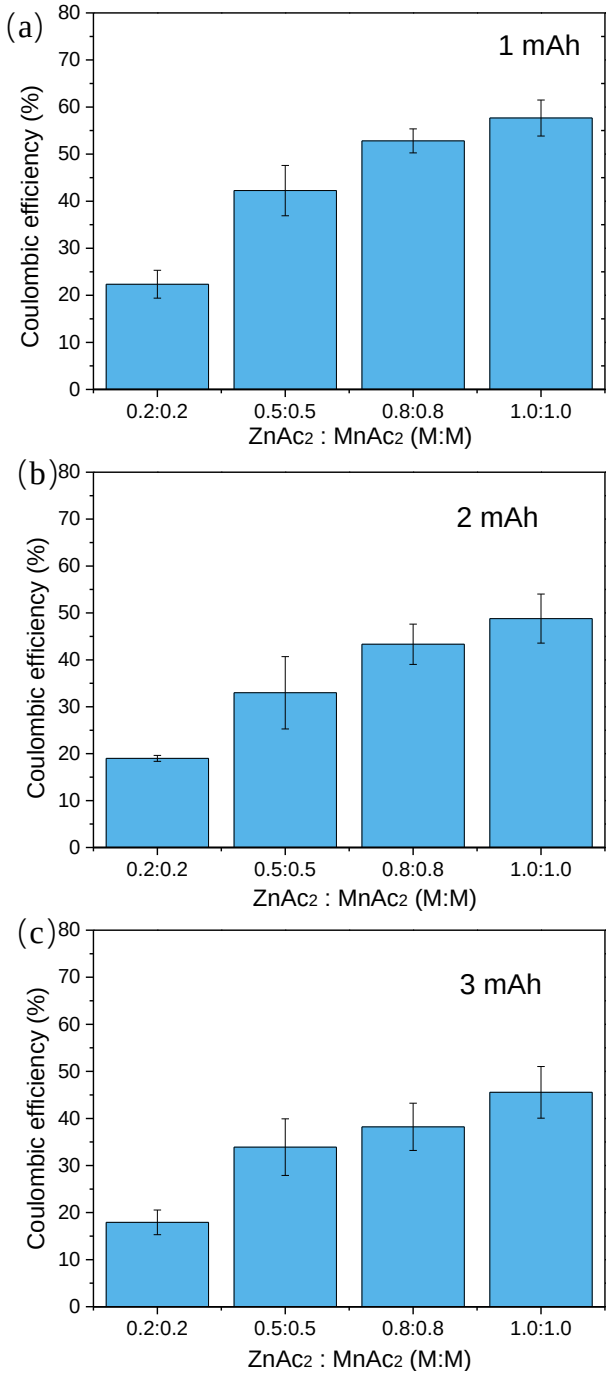

Fig. S10. The CEs of the thin-film carbon//carbon batteries based on electrolytes of x **M** $ZnAc_2$ + y **M** $MnAc_2$ + 0.1 **M** KI + 2 **M** KCl under 2 mA charge/discharge currents with charge capacity fixed as (a) 1 mAh, (b) 2 mAh and (c) 3 mAh. (x, y) = (0.2, 0.2), (0.5, 0.5), (0.8, 0.8) and (1.0, 1.0).

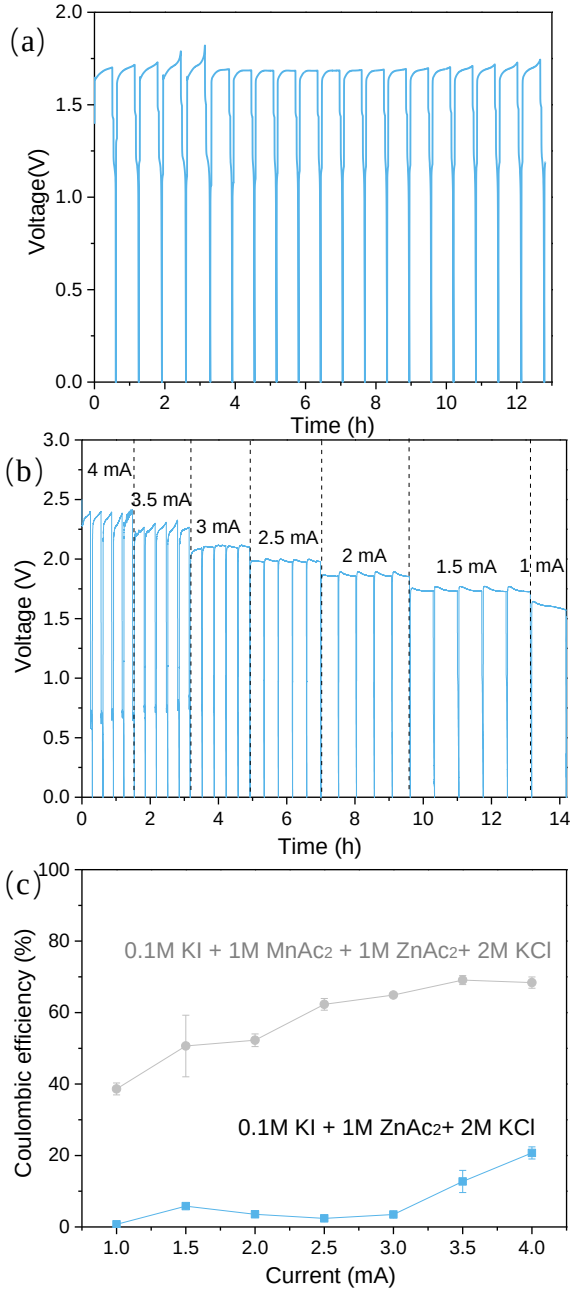

Fig. S11. The voltage curves of the thin-film carbon//carbon batteries based on electrolytes of 1 **M** $ZnAc_2$ + 0.1 **M** KI + 2 **M** KCl under (a) 2 mA and (b) different currents (1~4 mA) with fixed 1 mAh charge capacities. (c) CEs of (b) were compared with thin-film carbon//carbon batteries based on electrolytes of 1 **M** $ZnAc_2$ + 1 **M** $MnAc_2$ + 0.1 **M** KI + 2 **M** KCl.

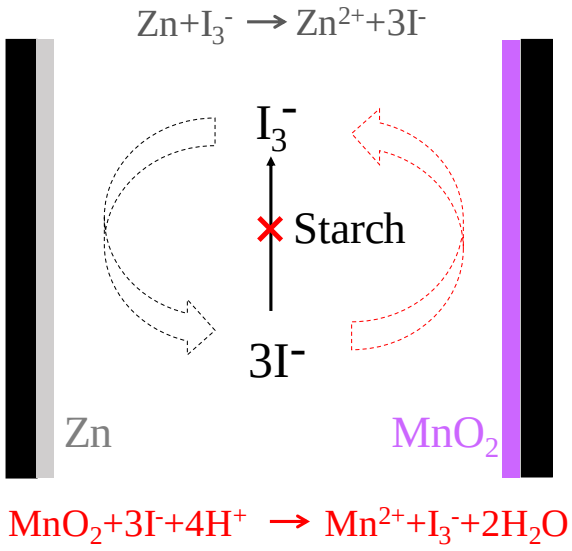

Fig. S12. Scheme of the reactions of mediator I^-/I_3^- with Zn and MnO_2.

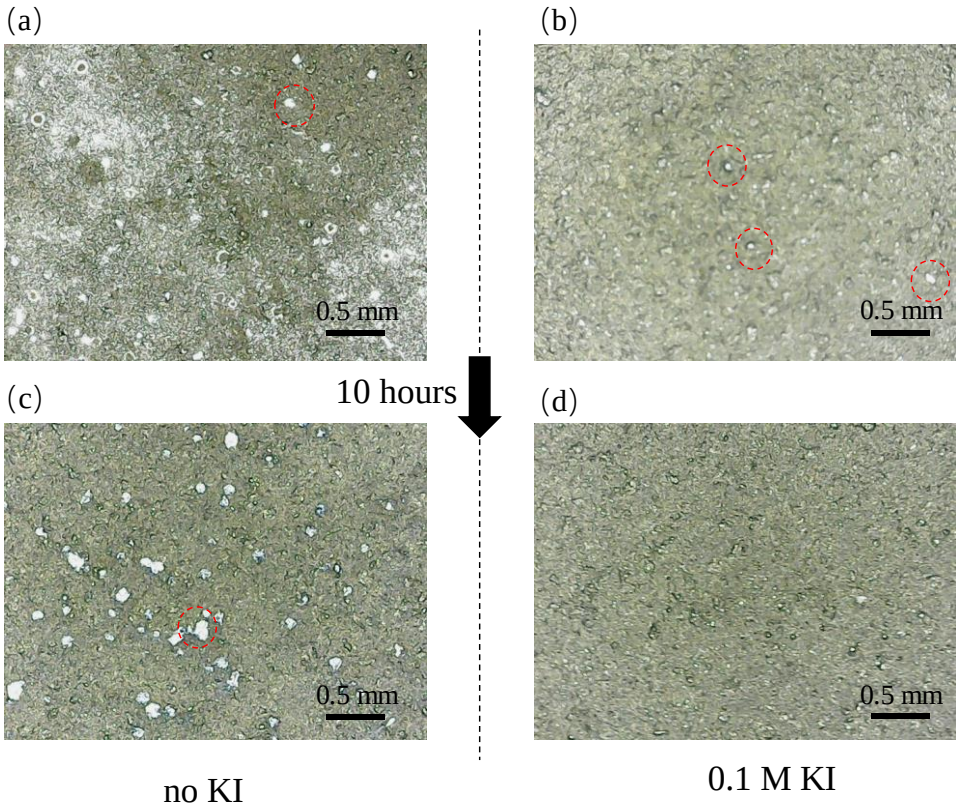

Fig. S13. The digital images of the anodes at the end of 1 mAh charge (a) without and (b) with 0.1 **M** KI, and then rest for 10 hours (c, d). The white deposit at anode side should be zinc metal after charging, which were lessened in the case with 0.1 **M** KI electrolyte additives.

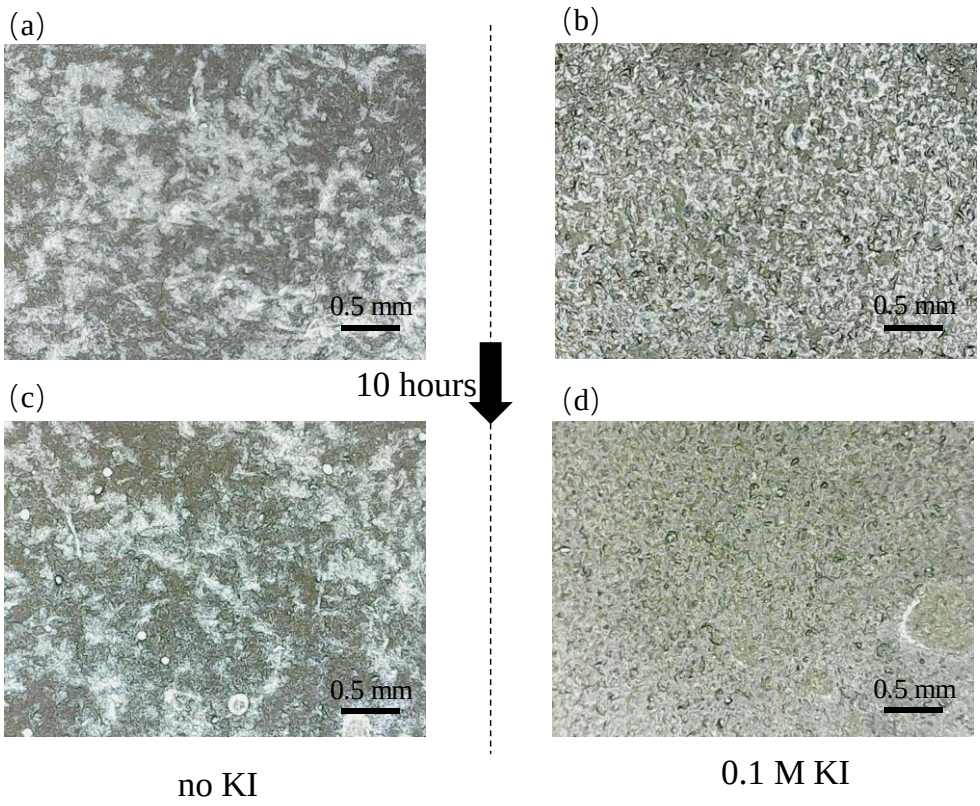

Fig. S14. The digital images of the cathodes at the end of 1 mAh charge (a) without and (b) with 0.1 **M** KI, and then rest for 10 hours (c, d). The white deposit at cathode side should be MnO_2 after charging, which were lessened in the case with 0.1 **M** KI electrolyte additives.

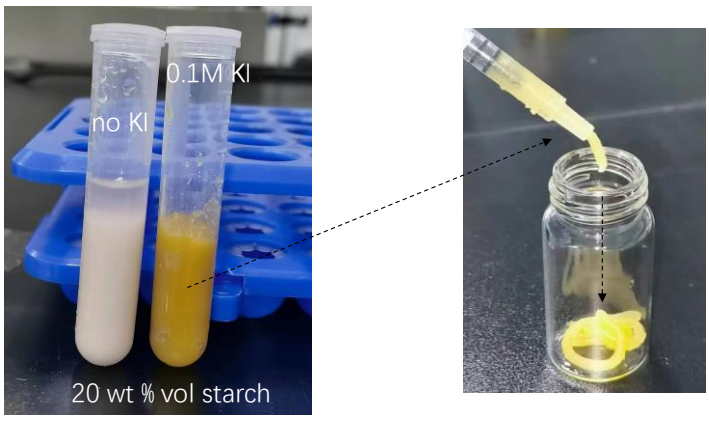

Fig. S15. Photos of the electrolytes of 1 **M** $ZnAc_2$ + 1 **M** $MnAc_2$ + 2 **M** KCl with and without 0.1 **M** KI after adding 20% (20 g in 100 mL) starch. While the electrolyte without KI did not gelate with starch, the electrolyte with KI showed good shape retention after adding 20% starch.

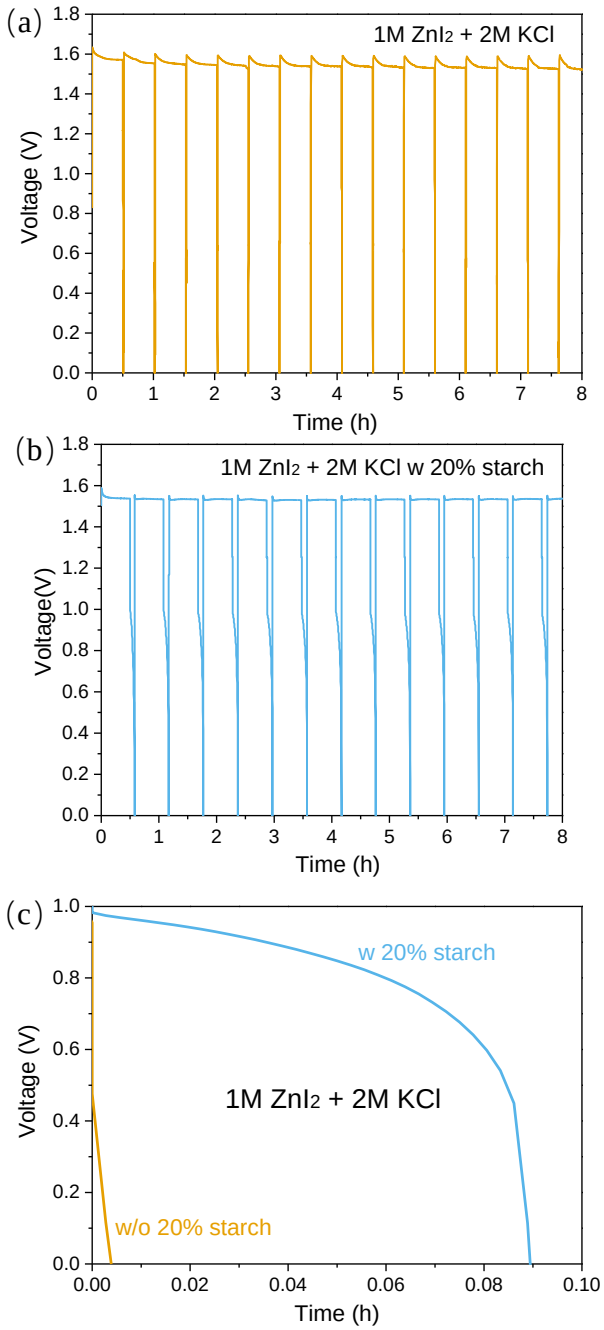

Fig. S16. The voltage curves of the thin-film carbon//carbon batteries based on electrolytes of 1 **M** ZnI_2 + 2 **M** KCl (a) without and with 20% starch. (c) Discharge curves in (a-b) were compared on one single cycle. The charge/discharge currents were 2 mA and the charge capacities were fixed as 1 mAh.

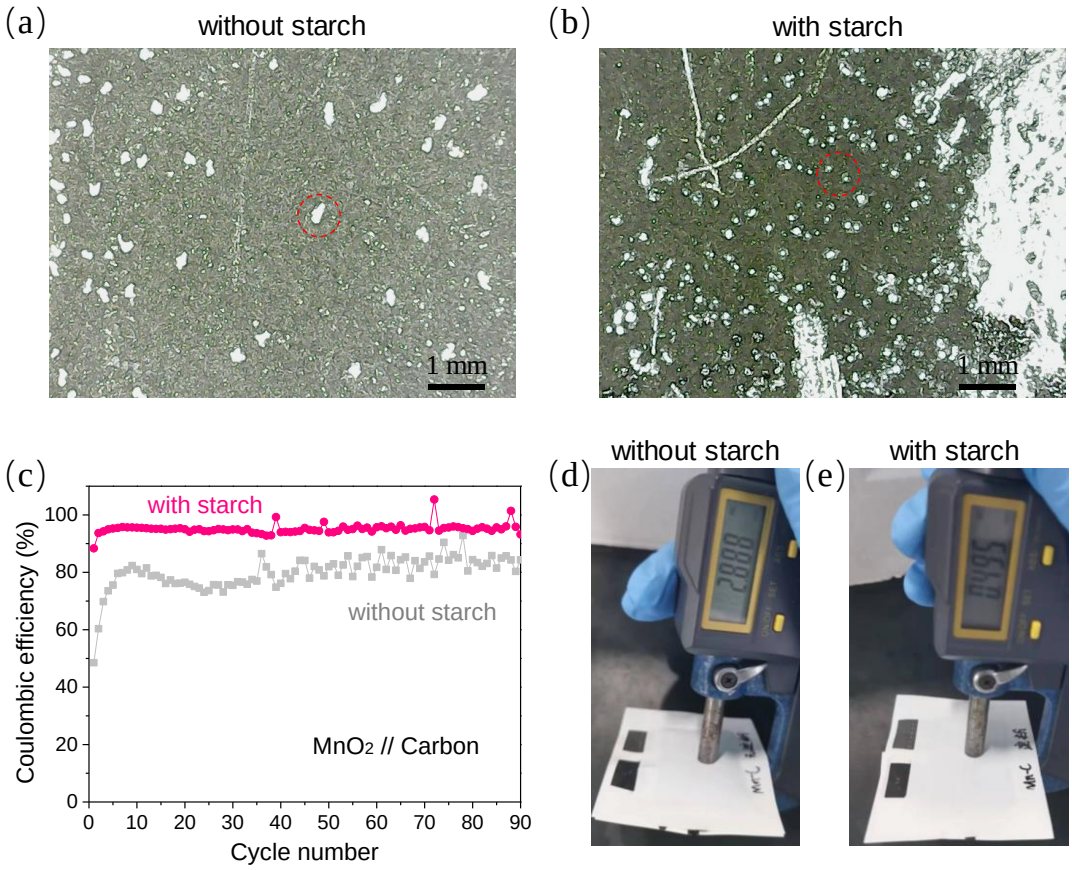

Fig. S17. The digital images of the zinc anodes at the end of 0.5 mAh/cm^2 charge (a) without and (b) with 20% starch. The white lump in (b) is the remain starch after gentle rinse with water. In the red circles, the size of zinc dendrites decreased after adding starch. After 90 cycles as shown in (c), the batteries based on electrolytes without starch (d) inflated, however, no obvious hydrogen evolution was found for batteries based on electrolytes after adding starch (e). The inflation test may prove the effect of starch on depress the hydrogen evolution. In addition, MnO_2 // carbon structure were applied for ruling out the factor of inefficient deposition of MnO_2.

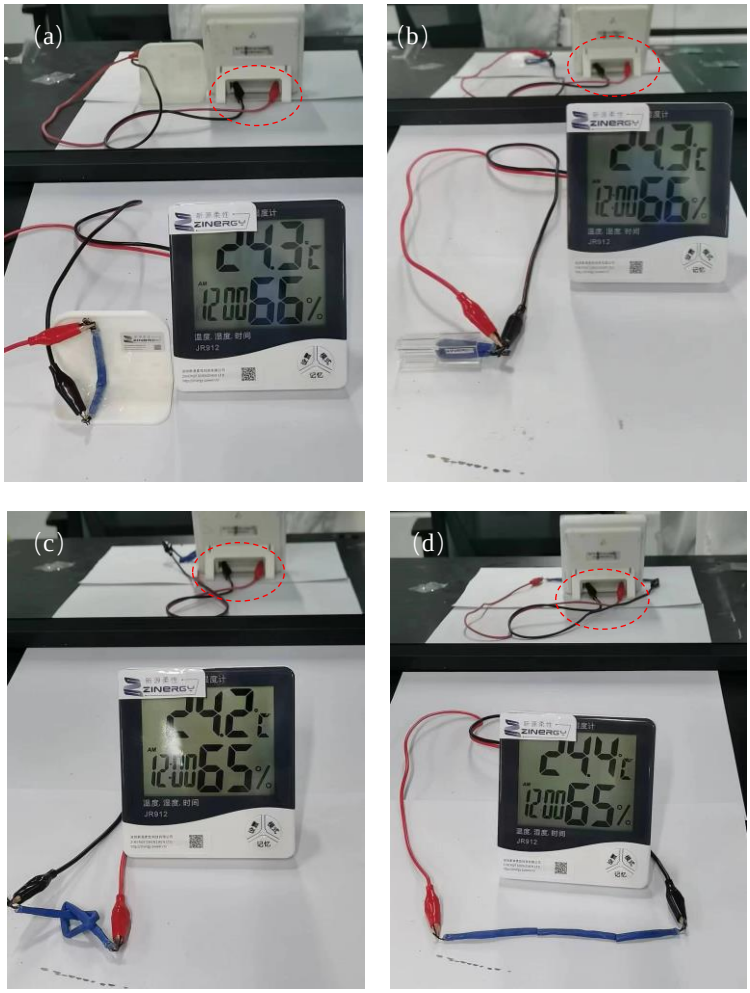

Fig. S18. Demonstration of flexibility and safety of the cable carbon//carbon batteries by (a) bending, (b) folding, (c) knotting and (d) cutting, where a mirror was put behind to prove the direct connection to the digital display meter. The electrolytes for the batteries were composed of 1 **M** $ZnAc_2$ + 1 **M** $MnAc_2$ + 0.1 **M** KI + 2 **M** KCl with 20% additional starch.

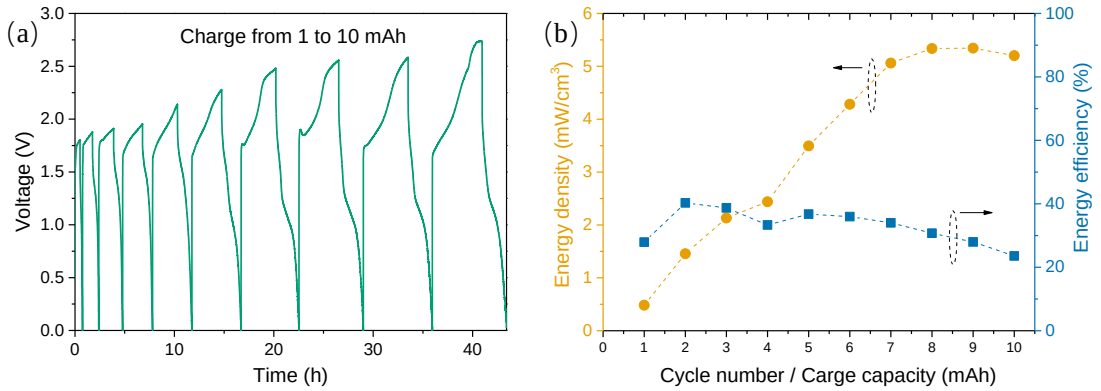

Fig. S19. (a) The voltage curves of the cable batteries under 2 mA current with charge capacities increased from 1 to 10 mAh. (b) The energy densities and energy efficiencies calculated from (a). The size of cable batteries: diameter of 0.46 cm and length of 6 cm, i.e. volume of 1 cm^3.

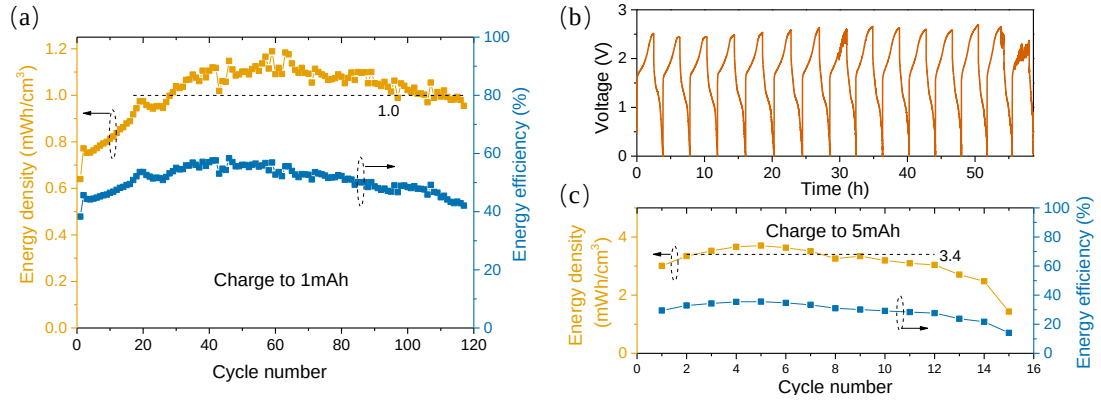

Fig. S20. (a) Energy densities and energy efficiencies of the straight cable battery in Fig. 4(b) under 2 mA charge/discharge current with charge capacities fixed as 1 mAh. (b) The voltage curves and (c) the energy densities and energy efficiencies of cable battery under 2 mA charge/discharge current with charge capacities fixed as 5 mAh.

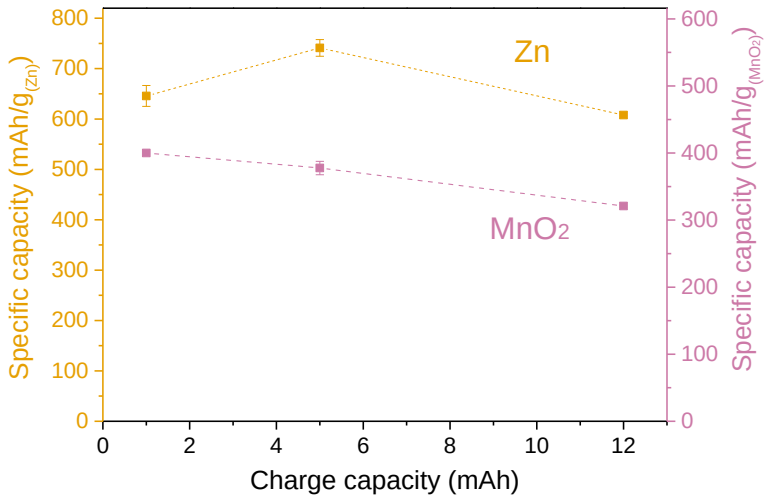

Fig. S21. The specific capacity of Zn and MnO_2 after charging with different capacities (1, 5 and 12 mAh) in cuvette batteries with 3 mL electrolytes. The specific capacities were estimated by dividing the deposited weight into the charge capacities. The deposited weights were obtained by vacuum drying the electrodes before and after charging. The electrodes were rinsed gently with water to clear the remain electrolytes after charging. Besides, the axes were scaled to the theoretical capacities of Zn (820 mAh/g) and MnO_2 (617 mAh/g) for better comparison.

Table S1. Summary of deposition weights and specific capacities of Zn and MnO_2 electrodes.

	MnO_2 deposited (mg)	MnO_2 capacity (mAh/g)	Zn deposited (mg)	Zn capacity (mAh/g)
1 mAh	2.5	400	1.55	645.8
5 mAh	13.24	377.6	6.75	741.1

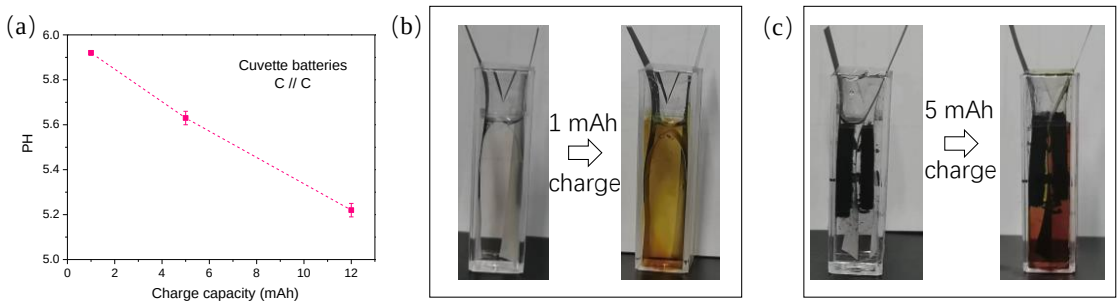

Fig. S22. (a) The PH value of electrolytes after charging with different capacities (1, 5 and 12 mAh). The photos of the cuvette batteries before and after charging at (b) 1 mAh and (c) 5 mAh. The volume of electrolytes is 3 mL. We note the volume of electrolyte in thin-film batteries is 250 uL, so 12 mAh charging capacity is for estimating 1 mAh in thin-film batteries cases. The decreased PH agrees with equation (2) $2MnAc_2 + 2H_2O - 2e^- \leftrightarrow MnO_2 + 4HAc + Mn^{2+}$, where HAc is generated during deposition of MnO_2. The darkening color of the electrolytes would be due to the generation of I_3^-.

Table S2. Comparison of electrochemical performance of the electrode-free zinc manganese battery in this work (marked bold) with the state-of-the-art Zn batteries (Zn^{2+} insertion into MnO_2, electrolytic MnO_2, fiber batteries).

	Anode side	Cathode side	Depth of discharge (DOD_{Zn})	MnO_2 capacity (mAh/g)	Energy Density (mWh/cm^3)
Cuvette battery	**Carbon felt**	**Carbon felt**	**3.44%**	**377.6**	**-**
Thin-film battery	**Printed carbon**	**Printed carbon**	**9.47%**	**400**	**-**
Cable battery	**Carbon rope**	**Carbon rope**	**4.93%**	**532**	**5.3**
Ref. [1]	Zn sponge	NiOOH	40%	-	-
Ref. [2]	Zn foil	α-MnO_2	-	285	-

Ref. [3]	Zn foil	β-MnO_2	-	225	-
Ref. [4]	Zn foil	Carbon cloth	-	556	-
Ref. [5]	Zn foil	Carbon felt	-	607	-
Ref. [6]	SS yarn @ Zn	SS yarn @ MnO_2	-	-	4.2
Ref. [7]	Zn spring	CNT sheet @ RuO_2	-	-	5.7

Note: The depth of discharge of Zn were estimated by the Zn^{2+} contents in the electrolytes in this work and the anode weight in ref. [1]. The MnO_2 capacity of cable batteries was estimated by the CEs of cable batteries (77.6%) and thin-film batteries (58.3%).

References

[1] J.F. Parker, C.N. Chervin, I.R. Pala, M. Machler, M.F. Burz, J.W. Long, D.R. Rolison, Rechargeable nickel-3D zinc batteries: An energy-dense, safer alternative to lithium-ion, Science 356(6336) (2017) 414-417.

[2] H. Pan, Y. Shao, P. Yan, Y. Cheng, K.S. Han, Z. Nie, C. Wang, J. Yang, X. Li, P. Bhattacharya, K.T. Mueller, J. Liu, Reversible aqueous zinc/manganese oxide energy storage from conversion reactions, Nat Energy 1(5) (2016) 16039.

[3] N. Zhang, F.Y. Cheng, J.X. Liu, L.B. Wang, X.H. Long, X.S. Liu, F.J. Li, J. Chen, Rechargeable aqueous zinc-manganese dioxide batteries with high energy and power densities, Nat Com 8 (2017).

[4] X.H. Zeng, J.T. Liu, J.F. Mao, J.N. Hao, Z.J. Wang, S. Zhou, C.D. Ling, Z.P. Guo, Toward a Reversible Mn4+/Mn(2+)Redox Reaction and Dendrite-Free Zn Anode in Near-Neutral Aqueous Zn/MnO(2)Batteries via Salt Anion Chemistry, Adv Energy Mater 10(32) (2020) 1904163.

[5] C. Zhong, B. Liu, J. Ding, X.R. Liu, Y.W. Zhong, Y. Li, C.B. Sun, X.P. Han, Y.D. Deng, N.Q. Zhao, W.B. Hu, Decoupling electrolytes towards stable and high-energy

rechargeable aqueous zinc-manganese dioxide batteries, Nat Energy 5 (2020) 440–449.

[6] J. Liu, N.Y. Nie, J.Q. Wang, M.M. Hu, J.H. Zhang, M.Y. Li, Y. Huang, Initiating a wide-temperature-window yarn zinc ion battery by a highly conductive iongel, Mater Today Energy 16 (2020).

[7] Y.F. Xu, Y. Zhang, Z.Y. Guo, J. Ren, Y.G. Wang, H.S. Peng, Flexible, Stretchable, and Rechargeable Fiber-Shaped Zinc-Air Battery Based on Cross-Stacked Carbon Nanotube Sheets, Angew Chem Int Edit 54(51) (2015) 15390-15394.